Dynamic Mechanical Relaxation and X-ray Scattering Study of Poly(butylene terephthalate)/Polyarylate Blends

Peter P. Huo† and Peggy Cebe*

Department of Materials Science and Engineering, Massachusetts Institute of Technology, Cambridge, Massachusetts 02139

Malcolm Capel

Department of Biology, Brookhaven National Laboratory, Upton, New York 11973

Received February 8, 1993; Revised Manuscript Received May 17, 1993

ABSTRACT: Blends of poly(butylene terephthalate) and polyarylate have previously been shown to be miscible for all blend compositions in the melt state or in the quenched amorphous state. Recently, we showed that all compositions of these blends exhibit depression of the thermodynamic melting point and a negative Flory interaction parameter.[1] Once PBT crystallizes, it will form crystal lamellae consisting of pure PBT and an amorphous phase of noncrystalline PBT and PAr. The composition of the amorphous phase is the subject of the present study. Dynamic mechanical analysis shows that there exist two tan δ maxima, indicating two amorphous regions, which are assigned to a mixed amorphous phase and a region primarily consisting of amorphous PAr. The location of the PAr depends on the blend composition and was studied by small-angle X-ray scattering (SAXS). For PAr composition <0.50, the long period of lamellar stacks, obtained from SAXS, increases as PAr composition increases, while for PAr > 0.50, it decreases. Lamellar thickness can be estimated from the breadth of (001) using wide-angle X-ray scattering. By combining the long period, lamellar thickness, and crystallinity, we derive a general methodology to describe the morphology of the blends. One main conclusion of this work is that the long period is strongly affected by the degree of undercooling. When blends of different composition are prepared with the same thermal history (i.e., the same T_c), their long periods will vary due to the different degrees of undercooling and competition between crystallization and phase separation. Our results show that, for PBT/PAr blends, interlamellar PAr structure holds for blends with PAr < 0.40, while either interfibrillar or interspherulitic structure exists for blends with PAr > 0.40.

1. Introduction

Polymer blends, due to the combination of two or more polymer properties, have been the focus of research for several decades.[2] The morphology controls the physical properties of polymer blends and then ultimately determines the usefulness of the polymer blends. We are particularly interested in one type of miscible polymer blend, where one polymer is amorphous and the other is crystallizable. Several of the most important blends available commercially are of this type.[3-10]

One such blend is poly(vinyl difluoride) (PVF_2)/poly(methyl methacrylate) (PMMA) which has been studied extensively.[3-9] Like poly(butylene terephthalate) (PBT)/polyarylate (PAr) blends, PVF_2/PMMA blends are miscible at all compositions in the melt. Dielectric relaxation spectroscopy shows that the interlamellar region is heterogeneous.[6] When PVF_2 crystallizes, phase separation occurs, forming PVF_2 crystal lamellae, a PVF_2 amorphous interphase, and a mixed PVF_2/PMMA amorphous phase. There is a layer of amorphous PVF_2 located nearest to the crystals in the interphase. Small-angle X-ray scattering indicates the remaining amorphous PVF_2, and all the PMMA is located further from the crystals in the interlamellar regions.[7] Theoretical considerations by Kumar and Yoon[11,12] indicate that the thickness and composition of the interphase are critically dependent on the Flory interaction parameter.[11,12]

Blends of PBT/PAr have been shown to be miscible at all compositions in the melt or in the amorphous state.[13-16] There exists a phase separation upon the crystallization of PBT, resulting in a crystal/amorphous lamellar structure.[14,15] Previously, it has been shown by dielectric relaxation spectroscopy[14] that the amorphous PBT and PAr are not mixed homogeneously. Our dynamic mechanical analysis of a PBT/PAr blend film also shows two relaxation peaks, indicating an amorphous phase heterogeneity. The two different amorphous regions represent the rejected PAr and crystal/amorphous interphase. Runt et al.[14] claimed that PBT/PAr blends have an interlamellar morphology just like PVF_2/PMMA blends. Their results were based on SAXS studies of blends with PBT composition higher than 0.50. They observed a linear increase in the long period of lamellar structure as a consequence of increasing PAr composition in the blends and concluded an interlamellar morphology. However, using the same thermal treatment for the blends does not mean their long-period variation can be ascribed solely to composition effects, since the long period will depend upon the degree of undercooling, and we have recently shown that the thermodynamic melting points for PBT/PAr blends are different.[1] Instead, we have to consider both the long-period, lamellar thickness and mass fraction of crystallinity. We develop a general methodology from geometric considerations for determining the structure of each blend individually by using the data from the SAXS, WAXS, and thermal analysis. We demonstrate that the morphology of PBT/PAr blends depends on the blend composition. For both melt- and cold-crystallized blends with PAr as the major component, a significant fraction of PAr is rejected from the interlamellar region.

2. Experimental Section

Poly(butylene terephthalate) was obtained from Polysciences. PAr was obtained from Amoco, with a 1:1 ratio of isophthalic and terephthalic units. Blends of PBT/PAr weight fractions 80/20, 60/40, 40/60, and 20/80 were made by following the method of Kimura et al.,[13] which involves coprecipitation from phenol/tetrachloroethane (TCE) into methanol. The quenched samples

† Present address: W. R. Grace Corp., Analytical Division, Columbia, MD 21045.

0024-9297/93/2226-4275$04.00/0

were made by heating the precipitates to 250 °C, holding for 60–90 s, compression molding, and then quenching in ice water. The quenched PBT and 80/20 blend show a little paracrystallinity, while quenched 60/40, 40/60, and 20/80 blends are purely amorphous. Melt-crystallized samples were prepared by heating the quenched film from room temperature to 250 °C for 1 min using a Mettler FP80 hot stage, then cooling quickly to the crystallization temperature T_c, and holding there for a time sufficient for completion of crystallization as required by the crystallization kinetics.[15,16] Cold-crystallized samples are obtained by heating the sample from room temperature to the temperature chosen and then annealing for some time. No evidence of transesterification was found from NMR studies of the samples we prepared this way.[17]

Furthermore, we used differential scanning calorimetry (DSC) to test the transesterification reaction at 250 °C. We scanned the 60/40 blend at 20 °C/min from room temperature to 250 °C, held there for a certain time ranging from 2 to 30 min, cooled quickly to room temperature, and then scanned again to 250 °C. This cycling procedure was repeated more than 10 times. The DSC scans show no difference for accumulated times (at 250 °C) shorter than 10 min but show a significant difference as the accumulated time approached 1 h. This indicates that the blend sample we prepared for 1 min at 250 °C has not undergone any significant transesterification reaction. It is also consistent with the previous report by Kimura et al., indicating that transesterification reaction is severe only after holding at 250 °C for more than 100 min.[13]

The glass transition temperature, melting points, and the endothermic heat of fusion were measured using a Perkin-Elmer DSC-4 at 20 °C/min. The sample weights were around 5-10 mg in order to achieve sufficiently precise heat of fusion and melting point measurements, and the precision of the sample weights was within 0.01 mg. Indium was used to calibrate the temperature and heat of fusion. We define DSC T_g as the midpoint of the glass transition region of the DSC at a scan rate of 20 °C/min. The total mass fraction crystallinity of PBT and PBT/PAr blends was obtained by using the ratio of the heat of fusion measured from the DSC endotherm area to that of perfect crystalline PBT, which is 34.0 cal/g.[18] Here, the mass used to normalize the endotherm area is the total sample mass of PBT and PAr. The partial mass fraction crystallinity is the crystallinity only within the PBT component in the blend and was obtained from the ratio of the total mass fraction crystallinity to the mass fraction of PBT in the blends.

Dynamic mechanical relaxation experiments were performed using a Seiko DMS 200 system with a heating rate of 2 °C/min and measurement frequencies from 1 to 50 Hz, under nitrogen gas flow. Sample lengths were 10 mm, and the cross-sectional areas were about 0.5 mm^2 with a measurement accuracy of 0.001 mm^2. Amorphous blends and semicrystalline samples, cold-crystallized at 180 °C for 30 min, were studied using dynamic mechanical analysis (DMA) over a temperature range from 0 to 220 °C. For dynamic mechanical relaxation, we define DMA T_g as the position of the maximum of the tan δ peak at 1 Hz.

Wide-angle X-ray scattering (WAXS) was used to determine the degree of crystallinity of the films. Films were examined in reflection mode using a Rigaku RU300 X-ray generator and a diffracted beam graphite monochromator. Cu Kα radiation was used with a step scan interval of 0.02° and a scan rate of 1°/min.

Small-angle X-ray scattering (SAXS) experiments were performed on both cold- and melt-crystallized samples at the Brookhaven National Synchrotron Light Source. The system was equipped with a two-dimensional position-sensitive detector. The sample-to-detector distance is about 120 cm, the X-ray wavelength was 1.28 Å, and the beam profile at the detector was treated according to pinhole geometry. Each SAXS scan was collected for 15 min. Due to the isotropic nature of our sample, circular integration of the SAXS intensity was used to increase the signal-to-noise ratio.

SAXS intensity has been corrected by subtracting the intensity from the background and from thermal density fluctuations, the latter of which can be obtained from the Is^4 vs s^4 plot.[19,20] Here, we simply assume that the scattering intensity from the thermal density fluctuation is constant. The long period is obtained by using the maximum peak position of the Lorentz-corrected intensity.[19,20]

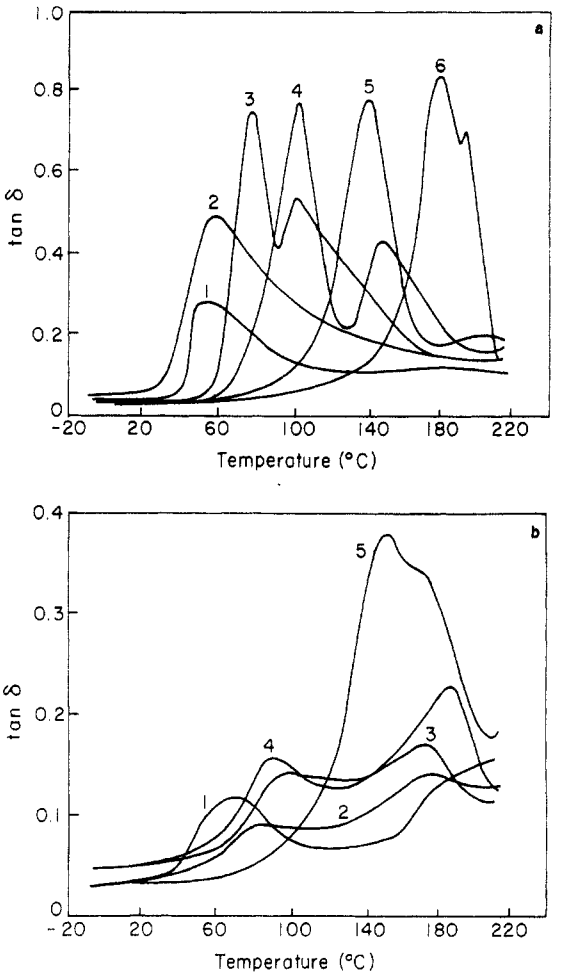

Figure 1. Loss factor, tan δ, as a function of temperature for PBT (1), PBT/PAr blends 80/20 (2), 60/40 (3), 40/60 (4), and 20/80 (5), and PAr (6): (a) quenched samples; (b) cold-crystallized samples.

3. Results

3.1. Dynamic Mechanical Behavior. We present tan δ as a function of temperature for all quenched samples in Figure 1a and for semicrystalline blends in Figure 1b. In Figure 1a, for PBT and 80/20 quenched samples, we only observe one broad asymmetric peak which has a steep increase to a maximum at 60 °C, followed by a long high-temperature tail due to a gradual reorganization of the poor crystals after further crystallization above T_g. Due to the very fast crystallization at lower temperature just above T_g for PBT and the 80/20 blend, very imperfect crystals form during the fast crystallization and are reorganized gradually into more perfect crystals over a wider range of temperature. The ability of quenched PBT homopolymer to reorganize during DSC scanning is shown in Figure 2. Here a cyclic test was used to study the thermal response at a slow scanning rate of 5 °C/min. The PBT was heated to 50 °C, then cooled and heated to 70 °C, then cooled and heated to 90 °C, and finally cooled and heated to 110 °C. Only the heating scans are shown. Immediately above the prior treatment temperature, shown by the vertical marker, the thermogram exhibits an exothermic departure. This indicates that the PBT is able to undergo an exothermic crystallization reaction on each successive scan. On this basis, we assign the high-temperature tail of the DMA scans of quenched PBT and 80/20 to constrained amorphous phase material in the reorganizing/recrystallizing films.

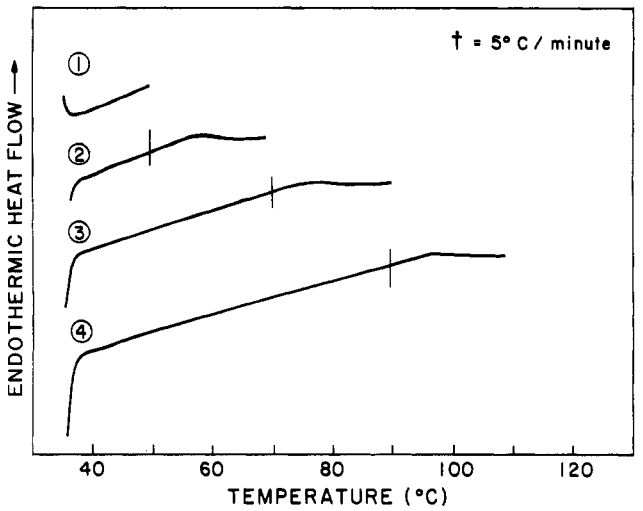

Figure 2. DSC thermograms of quenched PBT tested in a cyclic manner at ±5 °C/min. The thermograms show the heating cycle only. Film was heated to 50 °C (curve 1), then cooled and heated to 70 °C (curve 2), then cooled and heated to 90 °C (curve 3), and finally cooled and heated to 110 °C (curve 4). The vertical marker indicates the highest prior treatment temperature before each scan.

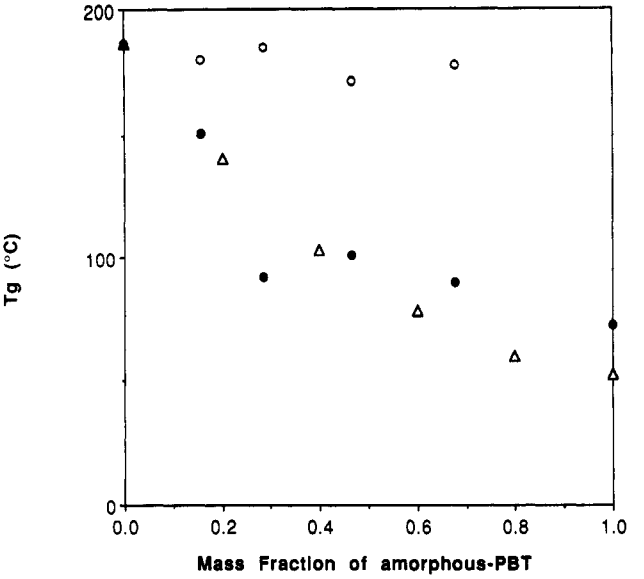

Figure 3. Glass transition temperature vs mass fraction of amorphous PBT. Determined by the DMA loss factor maximum for semicrystalline samples: lower T_g (●) and upper T_g (○). Determined by scanning calorimetry for quenched samples (Δ).

Both DSC and real-time SAXS results[16,21-28] support a recrystallization/reorganization model for quenched PBT and 80/20 blend. For 60/40 and 40/60 blends, we see a much sharper first peak followed by a second, higher temperature peak. The first peak at lower temperature is due to the relaxation of the amorphous chains in the amorphous sample, while the second higher temperature peak is due to the relaxation of constrained amorphous chains after crystallization. This is commonly seen in relaxation studies (either dielectric or dynamic mechanical) of other crystallizable polymers.[29,30] The 20/80 blend and homopolymer PAr show only one relaxation peak, which is then assigned as the T_g. The apparent double peak seen in the PAr sample is an artifact caused by the necking of the PAr sample at high temperature.

As is shown in Figure 1b, tan δ as a function of temperature for semicrystalline blends has a different appearance from that of the quenched materials shown in Figure 1a. For crystalline PBT homopolymer, we still observe one peak from the constrained amorphous phase in the semicrystalline sample, but the T_g or tan δ maximum is shifted to higher temperature compared with the T_g of the quenched PBT sample. But all other semicrystalline blends seem to have two tan δ maxima (hence, two T_gs). These are presented as T_{g1} and T_{g2} in Figure 3 together with DSC T_g for the quenched samples. (We were unable accurately to determine T_g of the semicrystalline samples using DSC because of the very small heat capacity increment.) As can been seen from Figure 3, the lower temperature T_g (T_{g1}), in general, has its value higher that the corresponding T_g for quenched blends, while the higher temperature T_g (T_{g2}) is quite independent of blend composition and is close to the T_g of the PAr homopolymer.

3.2. Wide-Angle X-ray Scattering. The WAXS intensity data shown in Figure 4 indicate that the quenched PBT sample is not 100% amorphous when compared to quenched blends 60/40 and 20/80 and to homopolymer PAr. Paracrystallinity is seen to exist in the quenched PBT sample and in 80/20 (which is not shown). All other quenched samples 60/40, 40/60 (not shown), 20/80, and PAr appear to be purely amorphous samples from the standpoint of WAXS. This is due to the much slower crystallization kinetics from the melt of PBT/PAr blends compared with PBT homopolymer, which permits blends

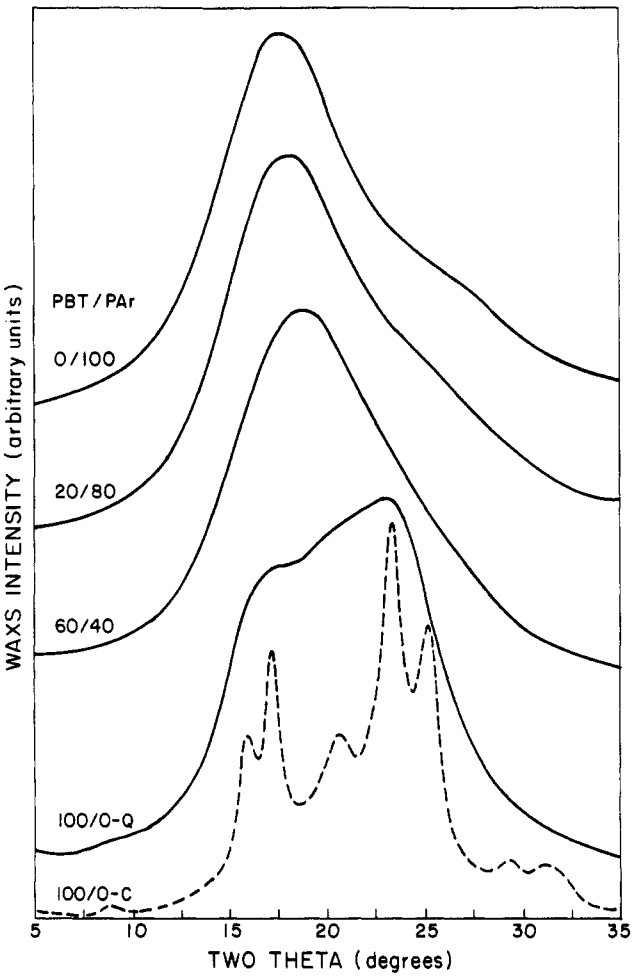

Figure 4. Wide-angle X-ray scattering intensity as a function of scattering angle, 2θ, for quenched PBT/PAr blends at the indicated compositions (solid lines) and for PBT homopolymer cold crystallized at 180 °C (dashed line).

with PAr greater than 20% to be quenched into the completely amorphous state. The semicrystalline samples exhibited very sharp peaks from the PBT crystalline phase. Cold-crystallized PBT is shown as an example in Figure 4 by the dashed curve. WAXS scans of the semicrystalline blends have been presented previously.[32,33]

Table I. Coherence Length in the a^*, b^*, and c^* Directions for Melt- and Cold-Crystallized PBT and PBT/PAr Blends

blend	a^* (Å)	b^* (Å)	c^* (Å)
	Melt Crystallized at 200 °C		
100/0	100	160	50
80/20	120	180	50
60/40	150	200	50
40/60	200	190	50
20/80	*a*	*a*	*a*
	Cold Crystallized at 180 °C		
100/0	80	120	40
80/20	80	120	40
60/40	130	150	40
40/60	150	140	40
20/80	*a*	*a*	*a*

[a] Not calculated.

We observed by solid-state ^{13}C NMR sharper resonant peaks in the well-crystallized blends compared with similarly well-crystallized PBT homopolymer.[17,31] This is a direct indication that the crystals in the blends are more perfect than those of PBT homopolymer. To estimate the crystal sizes in the crystallographic directions, we performed WAXS measurements for cold- and melt-crystallized blends in order to study the coherence length as a function of blend composition. Normal WAXS powder patterns were observed, and these have been shown previously.[32,33] Peak width has been shown to relate to the coherence length, t, by the Scherrer equation:[34]

$$t = K\lambda/\beta_{hkl}\cos\theta_{hkl} \quad (1)$$

where λ is the X-ray wavelength (1.54 Å), β_{hkl} is the half-width of peaks of Miller indices (hkl), θ_{hkl} is the scattering angle, and K is equal to 0.9.[34,35]

To determine the coherence lengths, we analyzed the (100), (010), and (001) peaks. We expect that the coherence length will not be exactly equivalent to the crystal size. The crystal lattice of PBT has been reported to be triclinic, with lattice parameters a = 4.83 Å, b = 5.96 Å, c = 11.62 Å, α = 99.9°, β = 115.2°, and γ = 111.3°.[36-38] However, the disposition of the unit cell within a crystal lamella has not yet been determined for PBT. Nonetheless, it is reasonable to assume that the c-axis may be nearly perpendicular to the lamellar crystal fold surfaces, and the coherence length determined from the (001) reflection may relate to the actual lamellar thickness. In any case, we assume that the PBT crystal lattice will be the same in the blends as in the homopolymer. The powder pattern from silicon was used to obtain the instrumental broadening factor. According to scattering theory,[34] when assuming a Gaussian line shape, we will have

$$B^2 = \beta^2 + b^2 \quad (2)$$

while assuming a Lorentzian shape would result in

$$B = \beta + b \quad (3)$$

where B is the experimental broadening, b is the instrumental broadening, and β is the real lattice broadening. The actual experimental case is intermediate between the two ideal cases above. The value of β can be obtained in a way described previously[34] and is then used to determine the coherence length from eq 1. In Table I, we list the calculated t. As can be seen from Table I, the coherence length in the a^* and b^* directions (determined from (100) and (010)) ranges from about 100 to 200 Å, depending on the blend composition. The lamellar thickness can be estimated from the (001) line broadening. The estimated lamellar thicknesses for PBT and blends are also listed in Table I. The lamellar thickness is about 50 Å for melt-crystallized samples and about 40 Å for cold-crystallized samples, independent of blend composition. The coherence lengths in the a^* and b^* directions are about 4–6 times that in the c^* direction. Due to very weak (001) peaks, we have relatively large error in estimating lamellar thickness, l_c, compared with that of the coherence lengths in the a^* and b^* directions.

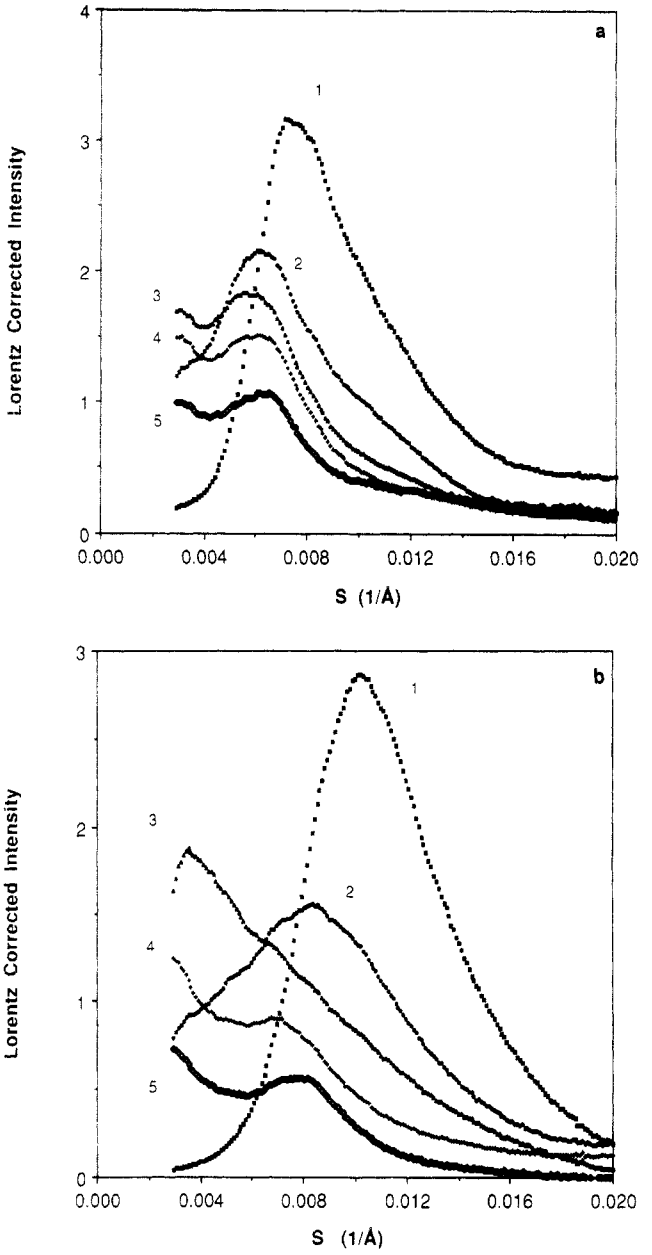

Figure 5. Lorentz-corrected SAXS intensity vs s for PBT and PBT/PAr blends numbered as in Figure 1: (a) melt crystallized at 200 °C and (b) cold crystallized at 180 °C.

3.3. Small-Angle X-ray Scattering. Room-temperature static SAXS has been done on both the cold-crystallized (T_c = 180 °C) and melt-crystallized (T_c = 200 °C) PBT/PAr blends. We obtain the long period from the Lorentz-corrected intensity maximum. The Lorentz-corrected intensity vs s data for the melt-crystallized blend samples are shown in Figure 5a. In Figure 5a, we found that the position of Lorentz-corrected intensity maxima of PBT/PAr blends increases for blends 80/20 and 60/40, but there is a decrease in the intensity maxima for blends 40/60 and 20/80. The same feature has also been observed for cold-crystallized PBT and PBT/PAr blends, which we show in Figure 5b. Now, the maximum for the 60/40 blend is not clear, and for this blend we barely see a shoulder instead of a distinct maximum. The long period L obtained from the intensity maximum as a function of the blend

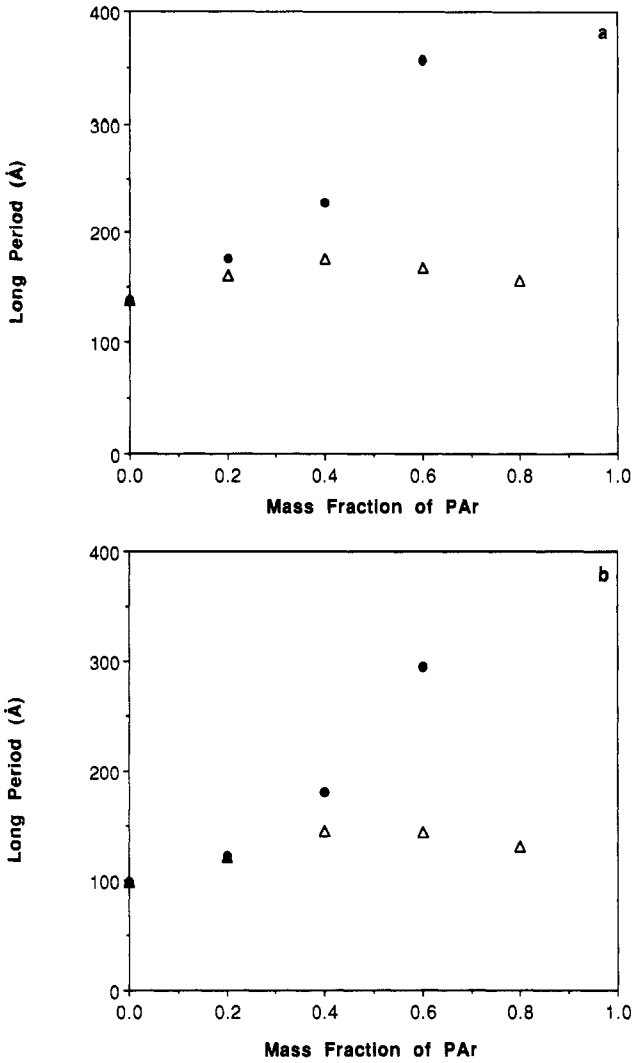

Figure 6. Long period as a function of the blend composition for PBT and PBT/PAr blends (Δ) measured and (●) calculated by assuming interlamellar structure: (a) melt crystallized at 200 °C, and (b) cold crystallized at 180 °C.

composition is shown in Figure 6a,b for melt- and cold-crystallized samples, respectively. The long period is nearly independent of the blend composition. For PBT homopolymer melt crystallized at 200 °C, the long period is 140 Å, while all melt-crystallized blends have long periods ranging from 160 to 180 Å. The cold-crystallized homopolymer and blends have long periods about 30 Å shorter compared with their melt-crystallized counterparts. The long period of cold-crystallized PBT homopolymer is 100 Å, while the long period of cold-crystallized blends clusters in the range 120–150 Å.

4. Discussion

The double T_g behavior for PBT/PAr semicrystalline blends indicates phase separation in the amorphous phase of the blends upon crystallization and is consistent with the previous report using dielectric relaxation spectroscopy.[14] Similar behavior has been reported for other blends, which are miscible in the melt or quenched amorphous states.[5,7] The number of separate glass transitions and their variation with composition depends upon the penetration ability of the amorphous polymer into regions occupied by the semicrystalline polymer. Different behaviors are observed for different blend systems. In PVF_2/PMMA, for example,[5] lower temperature tan δ maxima are independent of the blend composition, while the intensity of this maxima decreases as the PMMA

Table II. Lower and Upper Glass Transition Temperatures and Weight Fraction of Cold-Crystallized PBT/PAr Blends[a]

sample	T_{g1} (°C)	T_{g2} (°C)	$\tilde{W}_{11}$	$\tilde{W}_{21}$	$\tilde{W}_{12}$	$\tilde{W}_{22}$	W_{11}	W_{21}	W_{12}	W_{22}
80/20	90	178	0.81	0.19	0.06	0.94	0.66	0.16	0.01	0.17
60/40	101	172	0.69	0.31	0.10	0.90	0.43	0.19	0.04	0.34
40/60	92	185	0.78	0.22	0.01	0.99	0.28	0.08	0.01	0.63
20/80	151	180	0.26	0.74	0.05	0.95	0.13	0.38	0.02	0.47

[a] $\tilde{W}_{ij}$ = weight fraction of the ith component in the jth peak normalized for each peak, where $\sum_i \tilde{W}_{ij} = 1$. W_{ij} = weight fraction of the ith component in the jth peak normalized for the whole amorphous phase, where $\sum_{ij} W_{ij} = 1$. The indices are assigned as follows: i = 1 (PBT), 2 (PAr); j = 1 (lower peak), 2 (upper peak).

composition increases. This suggests that the lower temperature peak is from the pure PVF_2 amorphous phase. In this blend amorphous polymer cannot penetrate into the crystal/amorphous interphase. In other words, the interphase material consists only of purely amorphous PVF_2. For PBT/PAr blends, as shown in Figure 3, we observe a gradual increase of T_{g1} as the PAr composition increases, while T_{g2} is quite close to T_g of the PAr homopolymer.

Following the phase-separation analysis by Runt et al.,[39] we separate the phase component contributing to each T_g by assuming that each T_g follows the Fox equation.[40] The phase-separation results are shown in Table II. Several interesting observations can be made based on this separation. First, the higher temperature T_g, or T_{g2}, is mainly composed of PAr for all blends. The mass fraction of PAr contributing to the T_{g2} is about 0.90 or higher, which is very close to the total mass fraction of PAr. This implies that most PAr in the blends is phase separated and manifests its glass transition relaxation as T_{g2} in DMA. Second, the mass fraction of PBT contributing to T_{g1} is about 0.7–0.8, while only 0.2–0.3 PAr contributes to T_{g1}. This indicates that the first peak, T_{g1}, is mainly from PBT amorphous chains. But, with only DMA data, we cannot conclude whether the amorphous PAr placement is interlamellar, interfibrillar, or interspherulitic. To answer this question, we performed the SAXS studies described in section 3.3. In order to interpret our SAXS data, we needed crystal size information from WAXS which was described in section 3.2.

We conclude that the lateral dimensions of the crystals of the blends are slightly larger than those of PBT, while the lamellar thicknesses of the blends are almost the same as that of the PBT homopolymer. This is due to the significant reduction of crystallization rate upon adding amorphous polymer PAr into PBT. The slower crystallization rate at the same T_c for blends with different composition will result in formation of fewer nuclei for blends with higher PAr composition. This would then benefit the formation of large size crystals in such blends. For miscible blends, due to the presence of amorphous polymer, the crystallizable component crystallizes much more slowly than purely crystallizable polymer itself at the same T_c. This difference in kinetics could result in formation of larger and relatively more perfect crystals in the blends at the same T_c. Although there exists a melting point depression in these blends,[1] the experimental melting points do not necessarily decrease as a consequence of increased PAr in the blends. For melt crystallization at T_c = 200 °C, the observed melting points are 217.3 (PBT), 214.2 (80/20), 215.5 (60/40), 216.1 (40/60), and 217.5 °C (20/80).[1] In fact, this "strange" melting point behavior has been observed in other blend systems studied previously.[41] But after extrapolation to the thermodynamic

melting point via the Hoffman–Weeks plot,[42] we have found that the thermodynamic melting point of PBT homopolymer is actually higher than that of PBT/PAr blends.[1]

The long period increases as PAr composition increases for both melt- and cold-crystallized blends in which PBT is the major component. This is similar to the results reported by Runt et al.,[14] who studied the long period only for blend compositions containing PBT in proportion 50% or greater. But, they observed a much steeper increase of the long period as a function of the PAr composition. Despite the difference of our sample preparations, the long period of our melt-crystallized PBT (138 Å) is comparable to the results of Runt et al. of PBT (130 Å). But, we observe a much shorter long period for 80/20 and 60/40 compared with their blends of similar composition. For our data below 40/60 composition, we observe a decrease in the long period.

The DMA data show two T_gs, indicating phase separation in the amorphous phase region for PBT/PAr crystallized blends. Therefore, we need to determine the location of the PAr amorphous phase. The PAr may be in between the PBT crystal lamellae, forming the interlamellar structure, or it may form an interfibrillar or interspherulitic structure. The long period from SAXS has been used by several researchers in addressing the above issue.[14,43] When the long period is independent of the blend composition, previously it has been concluded that the structure is not interlamellar structure, while if the long period is a linear function of composition, interlamellar morphology is assumed.[14,43] Here, we must consider the meaning of comparison of the long period for blends crystallized using the same thermal history. For PBT/PAr blends, our previous results show that there exists a melting point depression.[1] The thermodynamic melting points are 249 (PBT), 246 (80/20), 242 (60/40), 236 (40/60), and 232 °C (20/80). Here, we observe a total 17 °C melting point depression from PBT to the 20/80 PBT/PAr blend. Choosing the same T_c indicates that a *different undercooling* is used for each different blend composition due to the different $T_m°$.[1] For PBT/PAr blends, at a melt T_c equal to 200 °C, the undercoolings are 49 (PBT), 46 (80/20), 42 (60/40), 36 (40/60), and 32 °C (20/80). It is well-known that the degree of undercooling is one of the key factors that determines the crystal lamellar thickness and linear growth rate.[44] In principle, by choosing appropriate undercooling, we could prepare any blend with a wide range in the long period. Also, due to the much different crystallization kinetics of PBT in the blends compared with the pure PBT, we would expect to be unable to make direct comparison among PBT and PBT/PAr blends. The difference in crystallization kinetics of blends compared to homopolymer has been reported previously.[15,16] Now, we conclude the trend of the long period as a function of the blend composition must be interpreted cautiously relative to morphology determination.

To determine if the morphology is interlamellar or not, one has to treat each crystallized blend individually by utilizing the long period, the lamellar thickness, and the (mass or volume) fraction of crystallinity. Other researchers have approached this problem by comparison of the linear crystallinity, from the one-dimensional electron density correlation function analysis, with the bulk crystallinity from calorimetry.[45,46] In our case, however, the extrapolation of the lower limit of the integral of the correlation function[47] to $s \rightarrow 0$ is hampered by the very large scattering we observe at low angles due to interference of large-scale structures. This low-angle scattering makes the evaluation of the correlation function difficult and compromises the calculation of the linear crystallinity. Therefore, we have chosen alternatively to use the comparison of the calculated long period with the measured long period for our evaluation of the validity of an interlamellar placement assumption for PAr.

Table III. Long Periods of Melt- and Cold-Crystallized PBT and PBT/PAr Blends

sample	measd L (Å)	calcd L (Å)[a]
	Melt Crystallized at 200 °C	
100/0	140	140
80/20	160	180
60/40	180	230
40/60	170	360
20/80	160	5000
	Cold Crystallized at 180 °C	
100/0	100	100
80/20	120	120
60/40	150	180
40/60	140	300
20/80	130	940

[a] Calculated assuming an interlamellar placement of PAr.

The long period L is compared with the ratio of lamellar thickness and total volume crystallinity, $v_{c,t}$. If $L = l_c/v_{c,t}$, we may conclude that the PAr location is interlamellar, while if $L < l_c/v_{c,t}$, the PAr location is interfibrillar or interspherulitic. Here the total volume fraction of crystallinity is obtained by the following:

$$\frac{1}{v_{c,t}} = 1 + \left(\frac{1-w_{c,p}}{w_{c,p}}\right)\left(\frac{\rho_1}{\rho_2}\right) + \left(\frac{x}{1-x}\right)\left(\frac{\rho_1}{\rho_3}\right)\frac{1}{w_{c,p}} \qquad (4)$$

where ρ_1, ρ_2, and ρ_3 are the densities of the PBT crystal (1.40 g/cm^3), amorphous PBT (1.28 g/cm^3), and PAr (1.21 g/cm^3),[13] respectively. x is the mass fraction of PAr in the blends, and $w_{c,t}$ and $w_{c,p}$ are the total and partial mass fractions of crystallinity, which are related by:

$$w_{c,t} = w_{c,p}(1-x) \qquad (5)$$

Here, the direct implication is that whether or not each sample has interlamellar structure for the PAr is decided only by its own long period, lamellar thickness, and mass fraction of crystallinity. There is no relation between different samples (either different blend compositions with the same thermal treatment or the same blend with different thermal treatment). It is therefore meaningless to show composition variation of all the long-period data for the purpose of deducing structure from the trend of L vs ϕ. The only criterion for concluding an interlamellar placement for the PAr is whether or not the observed long period is close to that calculated in the way shown above.

Knowing $v_{c,t}$ and the lamellar thickness, l_c, from WAXS and assuming an interlamellar structure, we show the calculated L in Figure 6a,b, as a comparison to the experimentally observed long period. The data are also tabulated in Table III. As described above, showing all data in the same plot does not indicate we can compare the blends one to another. Instead, we can only compare the experimentally observed long period with that calculated based on an assumption of interlamellar placement of PAr. For the 80/20 blend, the observed long period is close to that calculated, an indication that this blend has a structure close to interlamellar. For the 60/40 blend, there exists a significant difference between the observed and calculated long periods, indicating that a small portion of PAr is rejected from the region between the PBT lamellar crystals. As the PAr composition increases, the difference between observed L and calculated L increases.

For the cold-crystallized 40/60 blend, the observed long period (140 Å) is only half of that calculated (300 Å), and for the 20/80 blend the observed long period (130 Å) is much smaller compared with that calculated (940 Å). For these latter two blends, a significant amount of PAr has been rejected from the interlamellar region. A similar behavior has also been observed in the melt-crystallized blends.[48]

This can also been seen by considering the density of PBT and PAr. In terms of density data of crystal and amorphous PBT and PAr, we should expect a much stronger peak scattering intensity for blends compared with homopolymer PBT if we assume an interlamellar structure, since the blending of lower density PAr would increase the electron density contrast between PBT crystal regions and PBT/PAr amorphous regions. In fact, this is the case for PVF_2/PMMA blends previously studied by SAXS.[5] Contrary to what is expected for interlamellar PAr placement, for PBT/PAr blends the scattered intensity from the periodic structure *decreases* significantly compared with that of the PBT homopolymer, while the SAXS intensity at very low angle (near zero angle) is much stronger. This can be seen from Figure 5a,b. For PBT, we see the Lorentz-corrected intensity is close to zero at s near zero, reaching a maximum at $s = 0.01$ Å, and then decreasing to zero as s increases to infinity according to Porod's law. A strong intensity at small s ($s \rightarrow 0$) has been found for every blend (both melt and cold crystallized). The strong intensity at $s \rightarrow 0$ indicates that there exists a strong interference between large-scale structures. This has been observed in other polymer blend systems.[45,46] The larger structures are likely to be either spherulites or fibrillar bundles containing most of the PBT (both crystalline and amorphous) and very little PAr (amorphous) and another domain containing most of the PAr rejected from the PBT spherulites or fibrillar bundles.

Considering our DMA results shown in Figure 1b, we observed two T_gs for the semicrystalline blends, indicating an amorphous phase heterogeneity. One region of the amorphous phase has its T_g between that of PBT and PAr homopolymer, while another has its T_g very close to PAr T_g. The intermediate T_g region represents a mixed amorphous phase containing amorphous PBT and PAr. The region with T_g close to the PAr homopolymer indicates a much more homogeneous region containing PAr and little, if any, amorphous PBT. The first amorphous region is simply the crystal/amorphous interphase, while the second region is the amorphous region outside the crystal lamellae. Due to the lower density of the second amorphous region compared with that of the spherulites, there is interference between them, which accounts for the high scattered intensity at $s \rightarrow 0$.

Combining DMA, WAXS, and SAXS results, we have a clearer picture of the structure of PBT and its blends with PAr. For the PBT homopolymer, a simple lamellar structure is expected. For blends with lower PAr concentration, such as the 80/20 blend, the structure is close to the PBT homopolymer, forming an interlamellar structure. The PBT crystal lamellar thickness in the 80/20 blend is roughly the same value as that of the PBT homopolymer, but the long period increases due to 20% PAr located between PBT lamellae. For the 60/40 blend, part of the PAr is rejected from the PBT interlamellar region and furthermore from the spherulites or fibrillar bundles. This results in a slightly smaller increase in the long period compared with the long period calculated by assuming interlamellar structure. As the PAr concentration increases further, more and more PAr is rejected from the spherulites and a much smaller long period is observed compared with that calculated on the basis of an interlamellar structure. The segregation of amorphous polymer during crystallization from a miscible melt has been interpreted for the poly(ether ether ketone)/poly(ether imide) system by considering the relationship between the linear growth rate and the mutual diffusion coefficient between the components.[48] A similar study of PBT/PAr would be desirable and research along this direction is currently underway.

5. Conclusions

We have used dynamic mechanical relaxation and X-ray scattering to study blends of PBT and PAr prepared over a very wide composition range. Even at low compositions of PBT, the PBT crystallizes, forming phase-separated regions. In all crystalline blends we observe two glass transitions: the upper T_g is close to that of the PAr homopolymer, while the lower T_g shifts with composition. From DMA alone, we can conclude that there exists a region rich in PAr and a second region of mixed amorphous PBT and PAr. Using small-angle X-ray scattering, we find a large scattering intensity as $s \rightarrow 0$ in blends with a large PAr component. We conclude that this scattering arises from large-scale structure interference (spherulites or fibrillar bundles). In addition, we see strong coherent scattering from lamellar stacks.

Finally, we calculated the long period that would result from a purely interlamellar placement of PAr. This calculated long period is close to the measured long period only for low PAr composition. As the PAr composition increases, an interlamellar placement becomes less probable. For blends with PAr > 0.40 interfibrillar or interspherulitic placement of PAr is favored. One important conclusion of this work is that the placement of PAr cannot be deduced from the trend of the long period with composition. Instead, it is necessary to compare the measured long period to the calculated long period for each blend independently.

Acknowledgment. Research was supported by U.S. Army Contract DAAL03-91-G-0132. Research was carried out (in part) at the National Synchrotron Light Source, Brookhaven National Laboratory, which is supported by the U.S. Department of Energy, Division of Materials Science and Division of Chemical Sciences (DOE Contract No. DE-AC02-76CH00016). The authors thank Ingchie Kwan for the cyclic thermal analysis testing.

References and Notes

(1) Huo, P.; Cebe, P. *Macromolecules* **1993**, *26*, 3127.
(2) Porter, R. S.; Wang, L. H. *Polymer* **1992**, *33*, 2019.
(3) Nishi, T.; Wang, T. T. *Macromolecules* **1975**, *8*, 909.
(4) Wang, T. T.; Nishi, T. *Macromolecules* **1977**, *10*, 421.
(5) Rim, P. B.; Runt, J. P. *Macromolecules* **1984**, *17*, 1520.
(6) Hahn, B.; Wendorff, J.; Yoon, D. Y. *Macromolecules* **1985**, *18*, 715.
(7) Hahn, B. R.; Herrman-Schonherr, O.; Wendorff, J. H. *Polymer* **1987**, *28*, 201.
(8) Runt, J. R.; Barron, C. A.; Zhang, X. F.; Kumar, S. K. *Macromolecules* **1991**, *24*, 3466.
(9) Tekely, P.; Laupretre, F.; Monnerie, L. *Polymer* **1985**, *26*, 1081.
(10) Ito, H.; Russell, T. P.; Yoon, D. Y. *Macromolecules* **1987**, *20*, 2213.
(11) Kumar, S. K.; Yoon, D. *Macromolecules* **1989**, *22*, 4098.
(12) Kumar, S. K.; Yoon, D. *Macromolecules* **1991**, *24*, 5414.
(13) Kimura, M.; Porter, R. S.; Salee, G. *J. Polym. Sci., Polym. Phys. Ed.* **1983**, *21*, 367.
(14) Runt, J. P.; Zhang, X.; Miley, D. M.; Gallagher, K. P.; Zhang, A. *Macromolecules* **1992**, *25*, 3902.

(15) Runt, J. P.; Miley, D. M.; Zhang, X.; Gallagher, K. P.; McFeaters, K.; Fishburn, J. *Macromolecules* **1992**, *25*, 1929.
(16) Runt, J.; Gallagher, K. P. *Polym. Commun.* **1991**, *32*, 181.
(17) Huo, P.; Cebe, P. *Polym. Prep. (Am. Chem. Soc., Div. Polym. Chem.)* **1992**, *30* (1), 140.
(18) Illers, K. H. *Colloid Polym. Sci.* **1980**, *258*, 117.
(19) Glatter, O.; Kratky, O. *Small Angle X-ray Scattering*; Academic Press Inc.: New York, 1982.
(20) Koberstein, J. T.; Morra, B.; Stein, R. S. *J. Appl. Crystallogr.* **1980**, *13*, 34.
(21) Yeh, J. T.; Runt, J. P. *J. Polym. Sci., Polym., Phys. Ed.* **1989**, *27*, 1543.
(22) Nichols, M. E.; Robertson, R. E. *J. Polym. Sci., Polym. Phys. Ed.* **1992**, *30*, 305.
(23) Nichols, M. E.; Robertson, R. E. *J. Polym. Sci., Polym. Phys. Ed.* **1992**, *30*, 755.
(24) Cheng, S. Z. D.; Pan, R.; Wunderlich, B. *Makromol. Chem.* **1988**, *189*, 2443.
(25) Cebe, P.; Chung, S. *Polym. Compos.* **1990**, *11*, 265.
(26) Chung, J. S.; Cebe, P. *Polymer* **1992**, *33*, 2312.
(27) Chung, J. S.; Cebe, P. *J. Polym. Sci., Polym. Phys. Ed.* **1992**, *30*, 163.
(28) Huo, P.; Cebe, P.; Capel, M. *J. Polym. Sci., Polym. Phys. Ed.* **1992**, *30*, 1459.
(29) Boyd, R. *Polymer* **1985**, *26*, 324.
(30) Huo, P.; Cebe, P. *Macromolecules* **1992**, *25*, 902.
(31) Huo, P.; Cebe, P. *Macromolecules*, in press.
(32) Peszkin, P. N.; Schultz, J. M. *J. Polym. Sci., Polym. Phys. Ed.* **1986**, *24*, 2617.
(33) Desper, C. R.; Kimura, M.; Porter, R. S. *J. Polym. Sci., Polym. Phys. Ed.* **1984**, *22*, 1193.
(34) Kakudo, M.; Kasai, N. *X-ray Diffraction by Polymers*; Kodansha Ltd.: Tokyo, 1972.
(35) Kobayashi, Y.; Keller, A. *J. Mater. Sci.* **1974**, *9*, 2056.
(36) Yokouchi, M.; Sakakibara, Y.; Chatani, Y.; Tadokoro, H.; Tanaka, T.; Yoda, K. *Macromolecules* **1976**, *9*, 266.
(37) Mencik, Z. *J. Polym. Sci., Polym. Phys. Ed.* **1975**, *13*, 2173.
(38) Stambaugh, B.; Koenig, J. L.; Lando, J. B. *J. Polym. Sci., Polym. Phys. Ed.* **1979**, *17*, 1053.
(39) Rellick, G. S.; Rung, J. *J. Polym. Sci., Polym. Phys. Ed.* **1986**, *24*, 279.
(40) Fox, T. G. *Bull. Am. Phys. Soc.* **1956**, *1*, 123.
(41) Quintana, J. R.; Cesteros, L. C.; Peleteiro, M. C.; Katime, I. *Polymer*, **1991**, *32*, 2793.
(42) Hoffman, J. D.; Weeks, J. J. *J. Res. Natl. Bur. Stand.* **1962**, *66*, 13.
(43) Crevecoeur, G.; Groeninckx, G. *Macromolecules* **1991**, *24*, 1190.
(44) Hoffman, J. D.; Davis, G. T.; Lauritzen, J. I. In *Treatise on Solid State Chemistry*; Hanay, N. B., Ed.; Plenum Press: New York, **1975**; Vol. 3.
(45) Khambatta, B. B.; Warner, F.; Russell, T.; Stein, R. S. *J. Polym. Sci., Polym. Phys. Ed.* **1976**, *14*, 1391.
(46) Nojima, S.; Satoh, K.; Ashida, T. *Macromolecules* **1991**, *24*, 942.
(47) Strobl, G. R.; Schneider, M. *J. Polym. Sci., Polym. Phys. Ed.* **1980**, *18*, 1343.
(48) Hsiao, B. S.; Sauer, B. B. *J. Polym. Sci., Polym. Phys. Ed.*, in press.